Chapter 6

Investigating the microscopic origin of spin-reorientations in canted antiferromagnetic $SmFe_{3/4}Mn_{1/4}O_3$ orthoferrites

6.1 Introduction

The challenges facing technology for next-generation ultra-small/dense spintronic devices calls for multi-functional materials with extraordinary properties [180]. In this regard, enhanced understanding of canted antiferromagnetic systems and its spin re-orientation transitions (SRTs) are of the fundamental interest in condensed-matter physics. Rare-earth orthoferrites ($RFeO_3$) systems and its spin re-orientations, which are mainly manifested by accommodating the doped magnetic cations at R and Fe sites, proposed to be exceptionally important for technological implications [180].

Among the promising series of transition metal oxides, rare-earth orthoferrite $ReFeO_3$ compounds show extraordinary physical properties of spin-switching and spin-reorientations, tunable by the applied magnetic field and/or temperature [181], room temperature exchange bias [182]. These ferrites also exhibit magnetic [183], magneto-optic [184], and multiferroic [185] properties. Paradoxically, the ferroelectric properties of the rare-earth orthoferrite $SmFeO_3$ have been highly debated, and contrary reported [185, 186].

In this context, investigating, and understanding the underlying physics behind the origin of the these spin reorientation and influence of doping on these SRTs, and various

aspects of the magnetic/ferroelectric properties in transition metal oxide single crystals is a challenging and fascinating area of research in materials physics. Here, doping was made to tune the SRTs and ferroelectric properties of $SmFeO_3$ [187]. The co-existence of ferroelctricity and magnetism is very demanding topic for the next-generation energy-efficient data storage devices. However, enhanced understandings of nanoscale phenomenon further need to be established.

Recently, huge number of researches have been done about doped rare-earth orthoferrite [87], including R-site, and Fe-site to improve the physical properties of the host compound like crystal structure [88], magnetic structure [89, 90], electronic structure [91], photo-luminescence [92, 93], etc. Doping is the ultimate way to improve the device efficiency and stability and provide an effective way to modulate the inherent properties of doped perovskite nanocrystals, single crystals, and quantum dots. Doping means partial replacement/substitution the original constituent elements with targeted elements. For the case of solid solution, one have to chose dopant in such way to fulfill the Hume-Rothery rules [188] for the solid solubility. The parent compound $SmFeO_3$, shows a spin reorientation (SRT), *i.e.*, rotation of magnetization from the [001] axis above 480 *K* to the [001] axis below 450 *K*, known as the Γ_4 to Γ_2 transition [185] due to magnetic nature of rare-earth at high temperature, which is highest among the rare-earth orthoferrite family [83, 90]. Mn substitutes in B-site in order to tune SRT and understand the underlying physics and highly debated ferroelectric properties in the parent compound, which fulfill the criteria for the Hume-Rothery rule [188], and well known to tune magnetic structure from one phase to another phase. Interestingly, a new Mn-doping induce spin reorientation at lower temperature was successfully demonstrated.

In this Chapter, structural properties have been inferred from X-ray, electron diffraction, and single crystal laue diffraction data. Label and Rietveld refinement were performed with FullProf software [149]. Electron dispersive spectroscopic analysis had been done after the polycrystalline powder preparation and the single crystal growth to make sure the the presence of elemental compositions. Laue diffraction were used to orient the single crystals. By employing the dc magnetometery, various hidden properties of the canted antiferromagnetic phase in the Mn-$SmFeO_3$ single crystals were investigated. The experimental findings suggest that Mn-$SmFeO_3$ shows a new phase transition from week ferromagnetic to collinear antiferromagnetic, which is absent in parents compound on upon Mn-substitution under moderate external magnetic field at low temperature. Polarization (P) vs. electric field (E) confirming the week ferroelectric nature of SFMO single crystal on application of pooling field ± 3.5 T.

This chapter demonstrates that Mn-$SmFeO_3$ possess a large scale ground with a wide range of magnetism, and magneto-electric coupling possibilities at microscopic level.

6.2 Crystal structure

The family of rare-earth orthoferrites ($RFeO_3$), where R is rare-earth ion, crystallizes in the distorted orthorhombic perovskite structure with an orthorhombic unit cell, in Pbnm space group, which is a generic atomistic arrangements for many $RFeO_3$ perovoskite compounds [189, 190]. Fig. 6.1 illustrates the crystal structure for Mn-doped $SmFeO_3$ orthorhombic perovskite structure with space group Pbnm having the following distribution of ions in crystallographic positions: Sm^{3+} ions in (4c), Fe or Mn^{3+} ions in (4b) and O^{2-} ions in (4c) and (8d) as shown in Table 6.2 [190, 191]. The Fe^{3+} ions are arranged in FeO_6 octahedra, surrounded by six O^{2-} ions as detailed in Fig. 6.1, generated by VESTA software) [141], where blue, green, and violet sphere are corresponding to Sm, Fe/Mn, & O ions respectively. A single orthorhombic unit cell is highlighted and lines connect atoms to eye guideline having lattice constants as listed in Table 6.1.

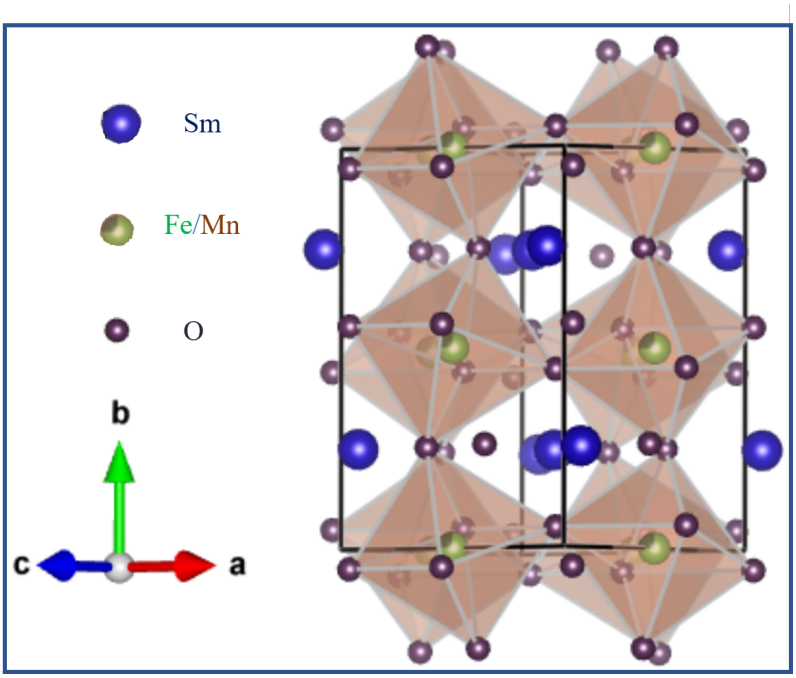

Fig. 6.1 Crystal structure of Mn-doped $SmFeO_3$ orthorhombic perovskite. The octahedra (FeO_6) are represented in light gray color to indicate the distortion in the Pnma structure.

6.3 Experimental details

6.3.1 Synthesis/Crystal Growth

The polycrystalline $SmFe_{0.75}Mn_{0.25}O_3$ (SFMO) powder samples were synthesized by the conventional solid-state rote with the High Energy Plenary Ball Mill method (System Inc., model Retsch-PM 400, Gmbh, Germany). The stoichiometric starting materials were of high purity Sm_2O_3 (99.99% of High Media), Fe_2O_3 (99.9% of Sigma Aldrich) and Mn_2O_3 (converted from MnO_2, *i.e.*, for the synthesis of Mn-doped $SmFeO_3$, one need Mn_2O_3 (manganese oxide (II)) but manganese dioxide, which is very cost effective, in contrast to MnO_2. So, for the conversion of MnO_2 to Mn_2O_3, study had adopted oxidation process of the Mn^{4+} into the Mn^{3+} in the presence of oxygen at 600 °C for 10 h).

The calculated amounts of powder was milled in ethanol medium for different period of time viz. 15 hours using zirconia jar and balls, and solid-state reaction air was done at 1300 °C for 12 h in a Ash furnace with 100 °C /hr heating and very slow cooling rate to avoid manganese deficiency. The phase quality of synthesized powder was confirmed by powder X-ray diffraction (PXRD) pattern [see Fig. 6.2] and the results are in good agreement with JPCDS file no. 741474.

The congruent polycrystalline feed and seed rods are considerably of high importance to obtain excellent quality of single crystal by optical float zone method. The feed and seed rods were prepared from the as-synthesized polycrystalline SFMO compound. The powder sample was ground and pressed into cylindrical rods, using a hydrostatic press at nearly 70 MPa pressure. The rods were then sintered at 1350 K for 20 h finally in the box furnace. The obtained seed rod having the diameter 5 mm and length 10 mm was utilized.

Single crystals of SFMO were grown in a four-mirror optical float-zone furnace (OFZF) (Crystal System Ins., model FZ-T-10000-H-HR-I-VPM-PC) using four 1 kW halogen lamps at IISER Pune. The proper assembling of feed and seed rods play an important role in the controlling of the growth process in the OFZF method. The temperature of the molten zone was carefully monitored by adjusting the power of the lamps. During the growth process, the molten zone moved upwards at a rate of 3-6 mm h^{-1}, with the seed and feed rod in sample holder stages called as lower shaft and upper shaft, respectively. Both are counter rotating at 20 rpm in air flow of 0.2 L min^{-1}.

6.3.2 Characterizations

The crystallinity and crystallographic analysis of powder samples were performed by X-ray diffraction (XRD), transmission electron microscopy (TEM), high resolution TEM

(HRTEM), and selected area electron diffraction (SAED). The structural analysis were performed with the powder X-ray diffractometer (Rigaku, Mini Flex 300/600, Japan, Cu K-radiation) with a scanning step of 0.02° and 2θ vary from 10° to 90°, and excellent phase quality has been also confirmed by the TEM (Tecnai G2 20 TWIN, FEI Company of USA (S.E.A.) PTE, LTD). The crystallinity and crystallographic directions were determined by X-ray Laue photography (Photonic Science) at IISER Pune. Surface morphology and composition of samples has been analyzed with the scanning electron microscopy electron dispersive X-ray spectroscopy (SEM & EDS, respectively).

The single crystals had typical dimensions of approximately 1.5 $\times$1.3 $\times$ 1.2 mm^3 having typical weight of 17.5 mg, used for the magnetic measurements. The temperature dependent bulk magnetic measurements were performed for the temperatures in the range of 10 K to 400 K and applied field strength up to H = 100 Oe parallel to a&c directions on single-crystal SFMO in ZFC (zero field cool)/FC (field cool) protocol, using the MPMS ®3 device (Quantum Design Inc.) system. M-H loop measurements were also carried out using the MPMS at various temperatures with applied magnetic field up to $\pm 4T$ along a and c axes. Special attention had been paid across the SRTs, in the range of 150K to 180K. The magnetic hysteresis data were collected across transitions in order to better understand the magnetic features. The magnetic measurements have been conducted on the samples that were fixed to quartz sample holders using diamagnetic glue.

6.4 Results and discussion

6.4.1 Powder X-ray diffraction

Fig. 6.2 Shows the X-ray diffraction pattern of nano particle of SFMO powder sample. The Rietveld refinement of the XRD data for SFMO sample was performed using FullProf program and shown in Fig. 6.2. The parameters I_{exp}, I_{cal}, and I_{exp}-I_{cal}, represents the experimental raw data, Rietveld fit calculated data, and difference between observed and calculated intensity of XRD pattern of SFMO sample, respectively. The experimental (red line), calculated (black line) and difference (blue line), and magenta vertical bars above the difference plot show the Bragg reflection positions. The diffraction patterns can be assigned to the single-phase orthorhombic perovskite structure and no impurity phases were detected, ensuring good quality of sample. The lattice parameters of SFMO powder sample, thus obtained are a = 5.3898(3) Å, b = 5.5979(3) Å and c = 7.6770(4) Å (χ^2= 2.5 %) as shown in Table 6.1, obtained with Rietveld refined XRD data. Here, few peaks are

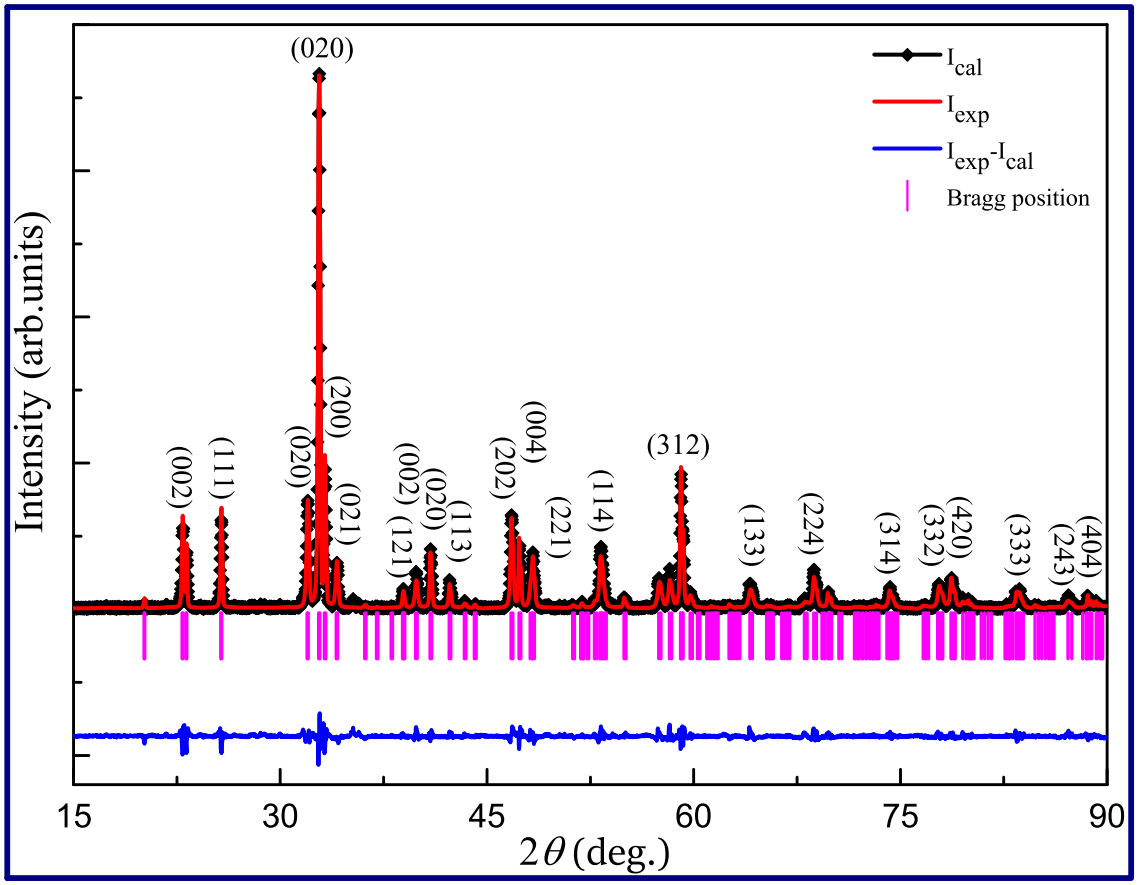

Fig. 6.2 Rietveld refined X-ray diffraction pattern for SFMO sintered at 1250 °C, the Observed (red line), calculated (black line) and difference between observed and calculated (blue line) XRD intensity profiles for SFMO obtained with Rietveld analysis using orthorhombic structure. Magenta vertical bars show the Bragg peak positions.

marked with (hkl) value just to show the planes obtained by SAED patterns are in well agreement with the XRD data.

Table 6.1 Structural parameters for bulk Mn-$SmFeO_3$

Lattice parameters	**a** (Å)	**b** (Å)	**c** (Å)
α=β=γ=90 (degree)	5.3898(3)	5.5979(3)	7.6770(4)
Wyckoff position	**x** (Å)	**y** (Å)	**z** (Å)
Sm (4c) (x,1/4,z)	0.98769	0.05631	0.25000
Fe/Mn (4b) (0,0.5,0)	0.00000	0.50000	0.00000
OI (4c) (x,y,1/4)	0.08587	0.47111	0.25000
OII (8d) (x,y,z)	0.75909	0.84403	0.05590
OIII (8d) (x,y,z)	0.66310	0.27249	0.46090

6.4.2 Transmission electron microscopy (TEM)

Fig. 6.3 shows the transmission electron microscope (TEM) micrographs and the corresponding selected area electron diffraction pattern (SAED) of SFMO nanocrystallites. The TEM image of the SFMO is shown in Fig. 6.3(a), indicating morphology of the crystallites as marked in inset. Fig. 6.3(b) illustrates the SAED data across the grain boundaries, displaying the crystalline nature of the SFMO sample. Fig. 6.3(c) shows the

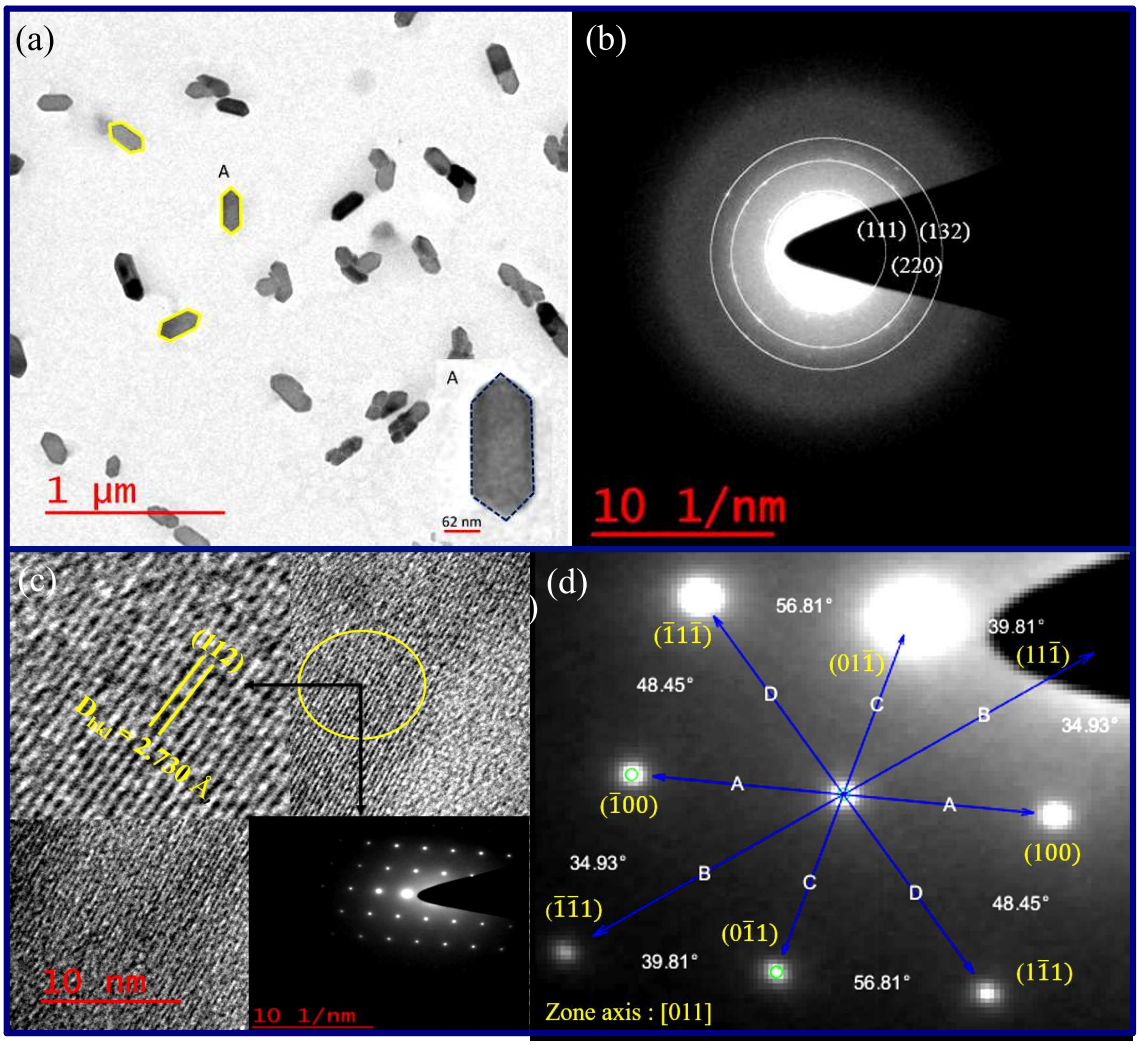

Fig. 6.3 TEM analyses of SFMO (a) TEM image of hexagon shaped SFMO crystallites (b) Shows the SAED pattern of particles obtained in TEM data Fig. 1(a), and (c) HRTEM micrographs of SFMO representing single domain, having no any defects, and upper inset show shows the enlarge view of under yellow circle area, whereas lower inset Fig. shows the SAED pattern of single domain. (d) Well indexed enlarged view of lower inset Fig.1(c).

HRTEM data analysis of SFMO nanocrystallites, revealing the clear visualization of single

domain pattern with the finite periodicity of align planes having inter-planar spacing (d_{hkl}) of 0.273 nm corresponds to the (012) plane. The obtained d_{hkl} value is comparable to estimated data from the XRD pattern. The upper inset shows the enlarge view of the lattice fringes corresponds to the circled area indicates high crystallinity of the SFMO nanocrystal. Whereas the lower inset shows the SAED pattern of under circle area, which shows the diffraction pattern having distinct and symmetric spots confirm the highly crystallinity of the single crystalline nanocrystal/single domain. Fig. 6.3(d) shows the enlarged view of the single crystalline SAED pattern, which is theoretical in well agreement for an orthorhombic crystal system and hold the d_{hkl} and R (distance between transmitted and diffracted beam) relation, and the angle between adjacent plan for the crystal system.

All the planes are indexed with CrysTBox software [174], which is theoretical in well agreement, and all the indexed planes are in agreement, and further confirms the crystal structure. In principle, it is in an agreement, if electron beam focus, in particular, one grain then it is oblivious to get a regular spot like diffraction pattern having inherent symmetry with the crystal system. And the crystallographic zone axis is estimated to be [011] that indicates single-crystalline SFMO nanocrystals growth direction, and all indexed planes correspond to the zone axis. These observations will play an important role in understanding the nanoscale phenomenon and an approach to play with single-crystal science at nano length scale. Since for a long time, it was believed that nanocrystallites were perfect single crystals, except at the surfaces, but the visualization of single grain can help to understand the properties of crystallites in a new way.

6.4.3 Energy dispersive X-ray (EDX) spectroscopy

Fig. 6.4(a) shows the SEM image of the SFMO powder sample to study its surface morphology. The SEM image indicates that the morphology of the particles is irregular because sintered sample being crushed until powder form is obtained. The SEM data also revealing the crystallites agglomeration due to the high surface activity and the magnetism. The EDS spectra was taken to confirm the composition of elements Sm, Fe, Mn, and O in the compound SFMO as shown in Fig. 6.4(b). The atomic % of the constituent elements are shown, which is in well agreement with the precursor compounds.

In order to make sure the elemental compositions of grown single crystals, the energy dispersive X-ray spectroscopy (EDX) were conducted. The experimental results are shown in Fig. 6.5, which are in well agreement with powder sample EDX spectra and litertaure. Indicates, there is no difficiency of oxygen and magnege and the experimental results shown in Fig. 6.4 & 6.5 are in good agreement.

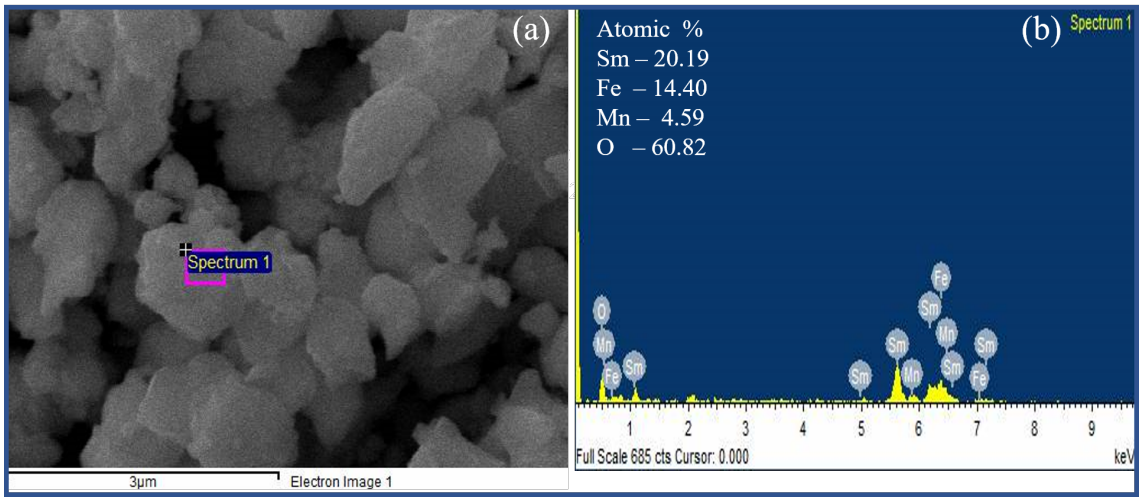

Fig. 6.4 SEM and EDS analysis (a) SEM micrograph of sintered ceramics SFMO at 1250 °C and (b) EDAX analysis of SFMO spectra of sintered ceramics SFMO at 1250 °C.

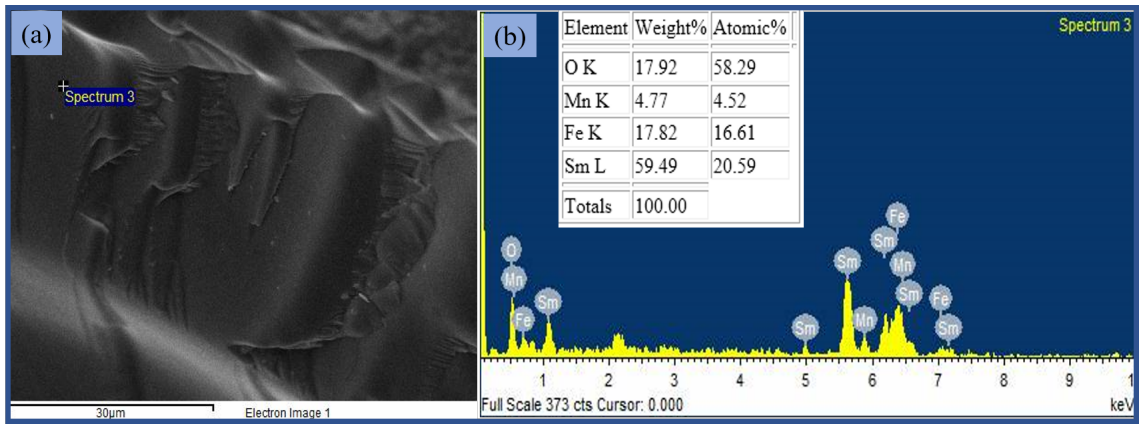

Fig. 6.5 SEM and EDS analysis (a) SEM micrograph of SFMO single crystal, and (b) EDX pattern of SFMO single crystal.

6.4.4 Single crystal Laue diffraction

The single crystal of SFMO, with 4 mm in diameter and 35 mm in length, was successfully grown with the optical float zone furnace, and the crystal exhibits shiny black surface, as shown in Fig. 6.6(a) along with the typical cut slice of ab plane in the form of disk. The crystallographic orientations and quality of the crystallinity was examined employing X-ray Laue diffraction. Fig. 6.6(b-d) shows Laue back-scattering patterns of SFMO single crystal along the (100), (010) and (001) crystallographic axes, respectively. The intense symmetric Laue diffraction spot pattern, indicates the high-quality of SFMO single crystal. Both XRD and Laue photography confirm the excellent quality of single phase SFMO

single crystal. The intense Laue pattern also indicates that the precisely cut align planes are perpendicular to the crystallographic axes.

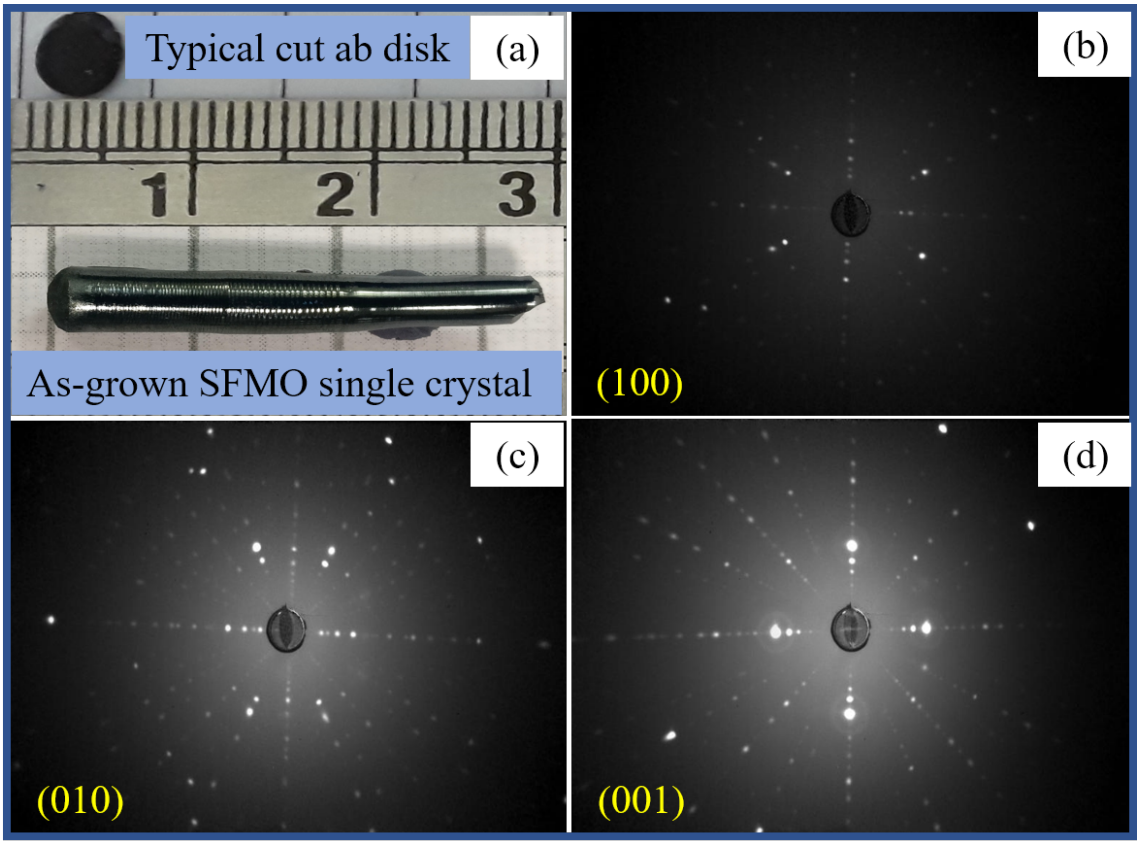

Fig. 6.6 (a) As-grown SFMO single crystal ingot (sample) and typical cut slice of a-b plane in the form of disk, and the crystal growth orientation in the ingot is along the crystallographic c-axis. (b-d) Laue back-scattering patterns of SFMO single crystal along the (100), (010) and (001) crystallographic axes, respectively.

6.4.5 Magnetic properties

In $RFeO_3$ family, these are the allowed spin configurations (Γ_1, Γ_2, Γ_3, Γ_4) [55, 56]. Namely, Γ_1 (A_x, G_y, C_z) represent the collinear antiferromagnetic nature with no net magnetization, and Γ_2 (F_x, C_y, G_z), Γ_3 (C_x, F_y, A_z), and Γ_4 (G_x, A_y, F_z) having week ferromagnetism along the a, b, and c axes, respectively, induced by canted antiferromagnetically coupled Fe moments [89, 90]. However, the parent compound $SmFeO_3$, shows a spin reorientation (SRT), *i.e.*, rotation of magnetization from the [001] axis above 480 K to the [001] axis below 450 K, known as the Γ_4 to Γ_2 transition (see Fig. 6.7) [185].

Fig. 6.7(a. b) shows the temperature dependence of magnetization for zero field cool (ZFC) and field cool (FC) protocol under a field of H = 0.01 T along a, b-axes for the $SmFe_{0.75}Mn_{0.25}O_3$ single crystal in the temperature range 10 - 400 K. The second order phase transition $\Gamma_4 \rightarrow \Gamma_2$ appeared at 390 K. The slight divergence in between ZFC and FC data might occur due to the stemming of ferromagnetic component either from a disorder-induced by Mn-doping or from a canted antiferromagnetic structure [192].

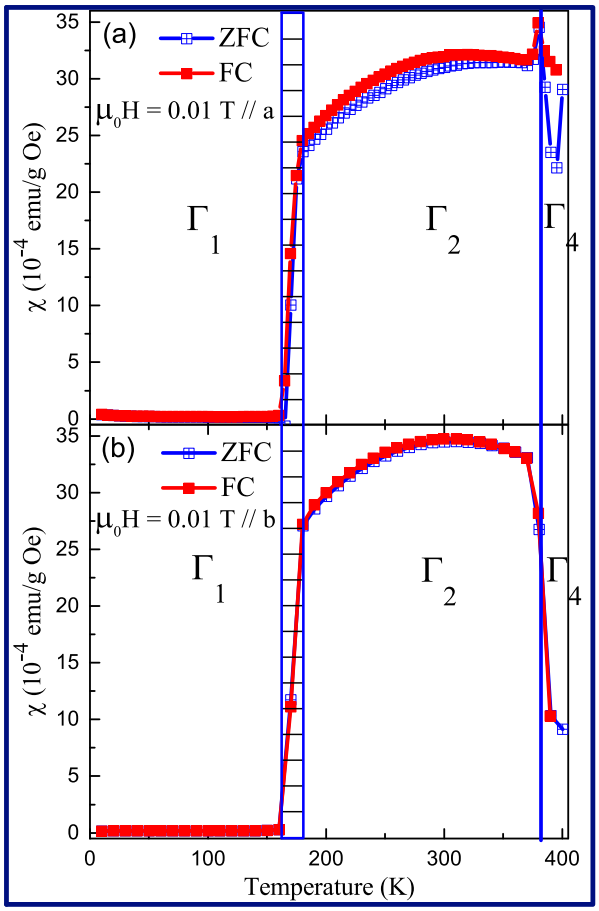

Fig. 6.7 Temperature-dependent magnetizations of SFMO single crystal in two protocol ZFC & FC along the a, b-axes at magnetic field H = 0.01 T.

Interestingly, a new feature of the magnetization curve is the another spin reorientation at T_{SR1} = 170 K, *i.e.*, the SFMO single crystal undergoes with weak ferromagnetism along a-axis (see Fig. 6.7(a, b)) to collinear antiferromagnet with no net magnetization, *i.e.*, $\Gamma_2 \rightarrow \Gamma_1$. The spin configuration from $\Gamma_2 \rightarrow \Gamma_1$ is due to Mn^{3+} doping in $SmFeO_3$ that gives a almost zero magnetic moment below T_{SR1} = 170 K [89]. Which is very rare for a rare-earth orthoferrite to possess a such a spin configuration (Γ_1), with the exception of $DyFeO_3$, for which the SR transition temperature (T_{SR} = 37 K) [193]. However Mn-doping

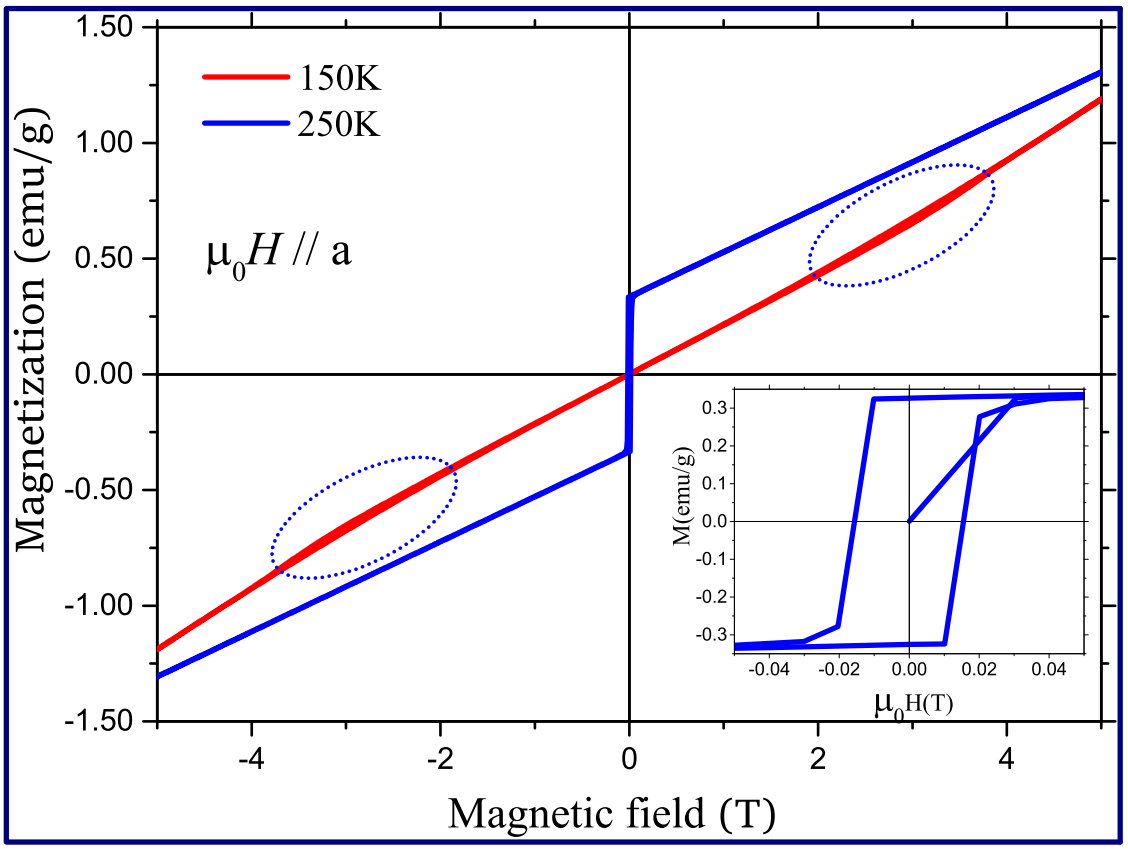

Fig. 6.8 Hysteresis curves for the SFMO single crystal along the a-axis at temperatures of 150 K, and 250 K. The inset Fig. of M-H at 250 K shows enlargement of the plot at the narrow range of magnetic field.

in Fe site is believed to be induce (Γ_1) spine configuration [89, 90]. The slightly divergence in between ZFC and FC data might be occur due to stemming of ferromagnetic component either from a disorder induced by Mn-doping or from a canted canted antiferromagnetic structure [192].

In order to study the spin reorientation further, the magnetic hysteresis curves were measured at temperatures (150 K & 250 K) along the a-axis with an applied magnetic field ranges in between $\pm$ 5 T as shown in Fig. 6.8. The M-H curve indicate the linear variation of magnetization. The opening in M-H at higher value of field nearly 3 T, indicates the canted nature of antiferromagnetic (AFM) ordering at 150 K. At higher temperature 250 K, the M-H curve shows the rectangular shaped of hysteresis corresponds to the weak ferromagnetic nature of SFMO single crystal along a-axis. A change of slope, corresponds to the spin reorientation configuration at 250 K can be seen from the inset Fig. 6.8. And the area marked under circled in Fig. 6.8 at temperature 150 K along the a-axis, which is

signature of canting along a-axis. Fig. 6.9 shows compensated AFM nature at temperature 150 K behavior along c-axis, having the noticeable kinks at temperature 250 K.

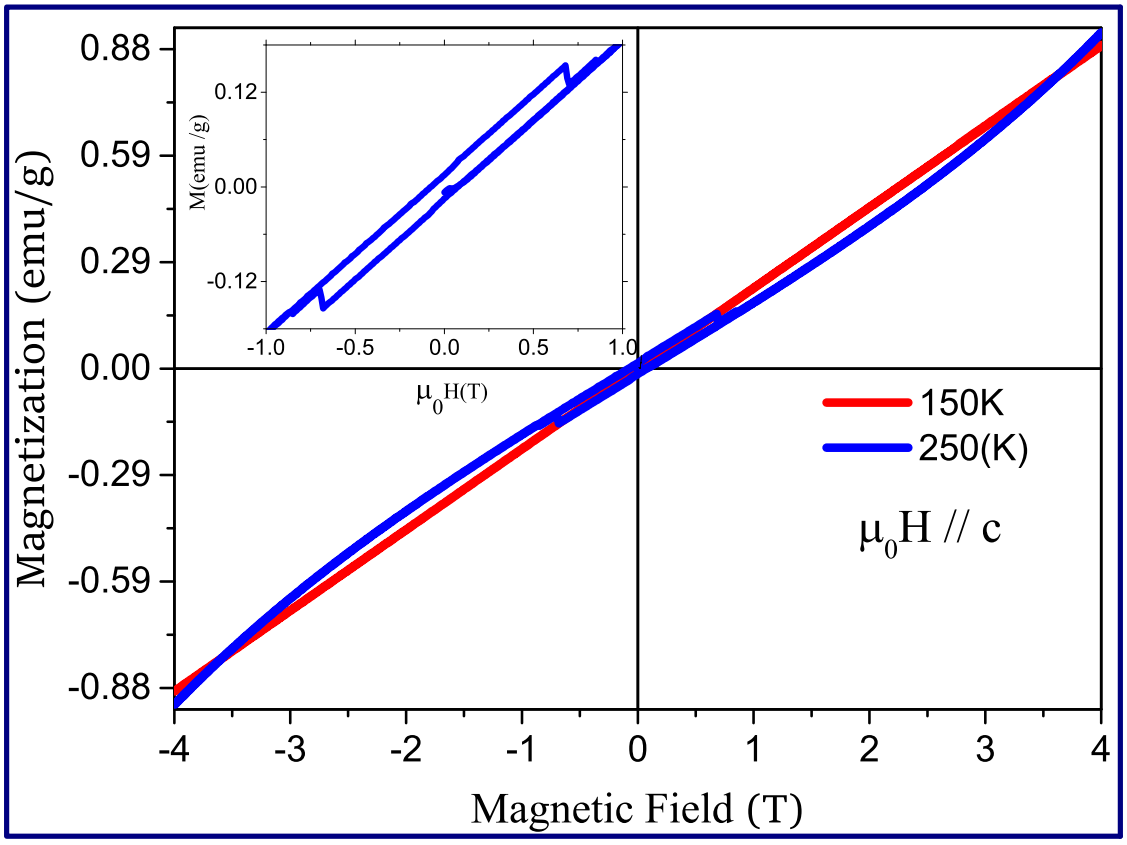

Fig. 6.9 Hysteresis curves for the SFMO single crystal along the c-axis at temperatures of 150 K, and 250 K. The inset Fig. of M-H at 250 K shows enlargement of the plot at small magnetic field.

Fig. 6.9 shows the magnetic hysteresis curves were measured at temperatures (150 K & 250 K) along the c-axis with an applied magnetic field ranges in between $\pm$ 4 T. The M-H curve indicate the linear variation of magnetization corresponds to the compensated antiferromagnetic (AFM) ordering at 150 K. At higher temperature 250 K, the M-H curve shows the with nominal opening in hysteresis corresponds to the canted AFM nature of SFMO single crystal along c-axis.

Additionally, M-H loops were recorded for a applied magnetic field $\pm$1000 Oe along a-axis and $\pm$1500 Oe along c-axis at various temperatures (140 K, 150 K, 160 K, 165 K, 170 K, 175 K, 180 K, 200 K), as shown in Fig. 6.10(a-d). Although magnetic M-H loops were already studied by Kang *et al.* [89], in the present investigation a systematic study across the transition was carried out. Fig. 6.10 shows canted antiferromagnetic spin structure up to temperature 160 K. As the temperature was increased from 160 K, it indicates the emergence and enlargement of domain state of the SFMO single-crystal. The results shows

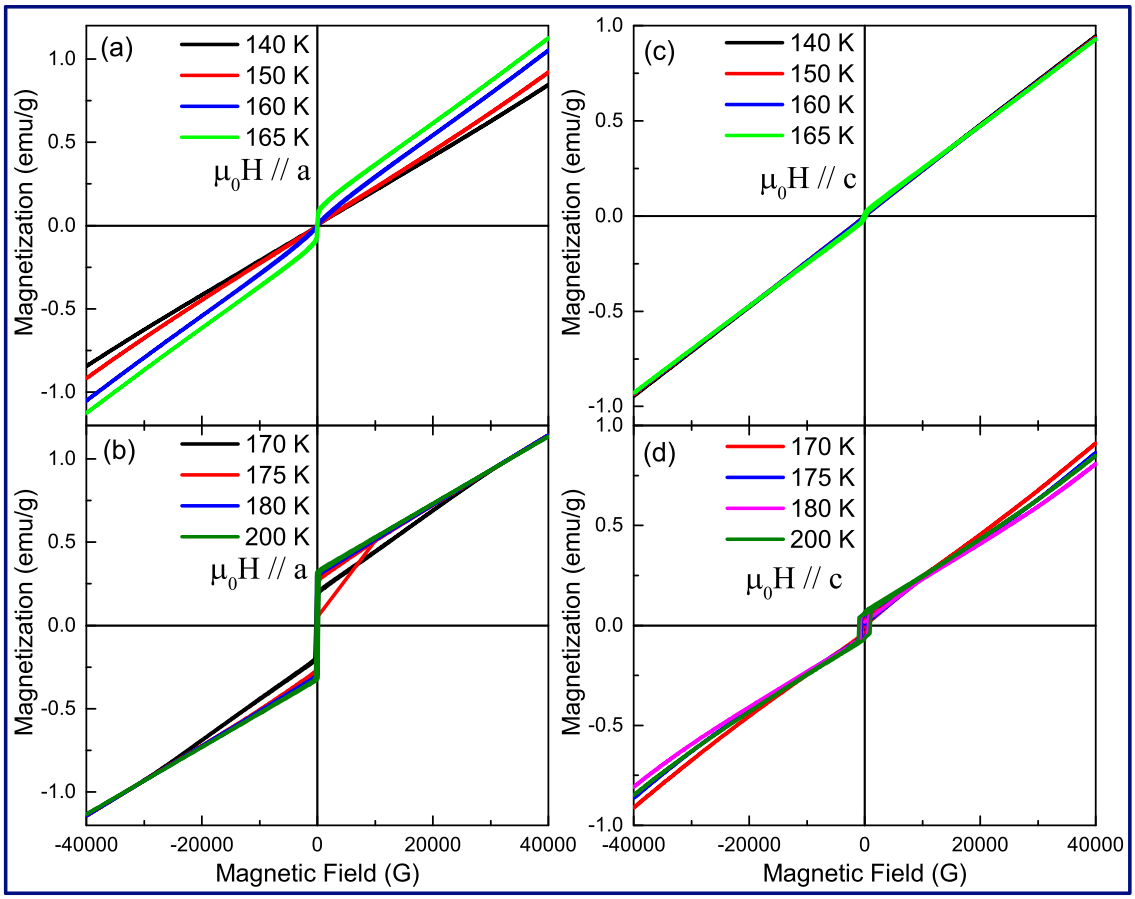

Fig. 6.10 (a, b) M–H curves for the SFMO single crystal along the a-axis at various temperatures in the range of 140 K to 200 K, and (c, d) M–H curves for the SFMO single crystal along the c-axis at various temperatures in the range of 140 K to 200 K.

the transtion from collinear to week ferromagnetic spin order beyond the temperature nearly 160K. The rectangular M-H loops have been recorded, with the characteristic of week ferromagnetic state, indicates the coercivity and remnant magnetization goes to increases upon increasing the temperature. However, Fig. 6.10(a) is in well agreement with the Fig. 6.10(c) in low temperature regime. Whereas, Fig. 6.11(b) slightly change in hysteresis nature of SFMO single crystal with respect to crystallographic c-axis at high temperature regime as shown in Fig. 6.11(d). The hysterics elements are vary in accordance with temperature as shown in Fig. 6.11(b, d).

The temperature variation of H_C in both ($\pm$) quadrant along a, c-axes is shown in Fig. 6.11(a-b) shows the visual transition at temperature 165 K, and beyond this value of temperature coercive filed will goes to enhanced gradually along both the crystallographic orientations. Both the Figs. are differ by the value of exchange bias, which is 100 Oe along a-axis and very nominal along c-axis in contrast to step size.

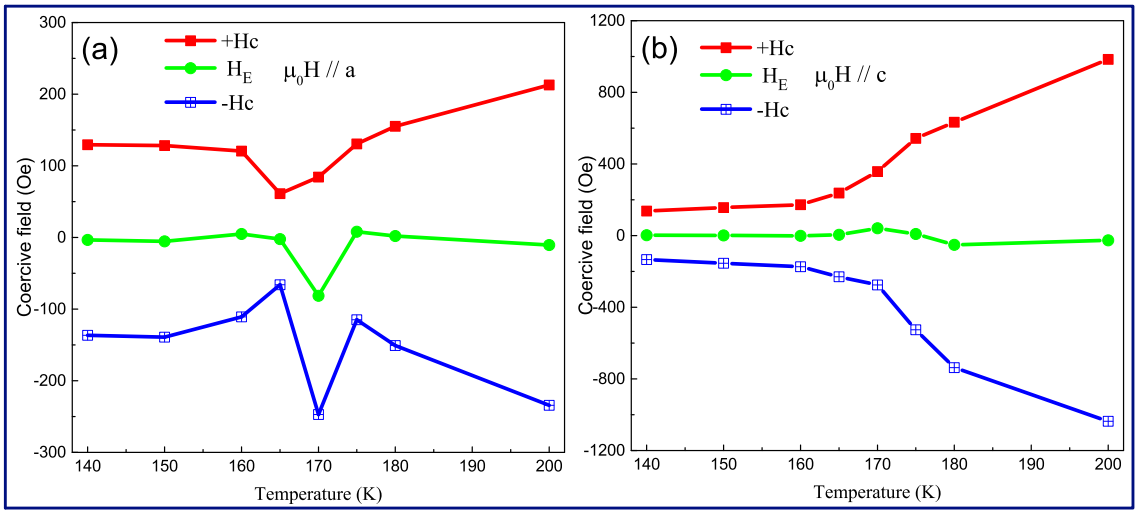

Fig. 6.11 (a and b)Temperature dependence of the exchange bias (H_E) along a, c-axes, and the coercivity H_c in both positive and negative quadrant is measured on the SFMO single crystal.

6.4.6 X-ray absorption spectroscopy

The element specific properties of SFMO were also studied by linear polarization-dependent Sm-M and Fe-L edge X-ray absorption spectra (XAS), conducted at PM3, BESSY-II (HZB), Berlin, Germany beamline with ALICE diffractometer. The element specific spectra were recorded in the total electron yield mode. The polarization-dependent Fe-$L_{3,2}$ and Sm-$M_{5,4}$ XAS spectra at room temperature with the propagation vector of light being in (a-c) plane are shown in Fig. 6.12(a, b). Fig. 6.12(a) shows the two intense peaks of Fe L_2 and L_3 multiplets resulting due to spin-orbit coupling that are assigned to Fe 2p→3d states. The intensity of the peaks is designated to the unoccupancy of Fe (3d) states [121, 123].

The L_3 (712.10 eV, Fe $2p_{3/2}$) and L_2 (725.31 eV, Fe $2p_{1/2}$) the features of L_3 is composed of a low intense peak marked as t_{2g} (Fe $2p_{3/2}$-t_{2g}) and the main peak assigned as e_g (Fe $2p_{3/2}$-e_g). As the multiplet structure of 3d metals and its X-ray spectroscopic assessment are generally well understood and provide a versatile tool for the atoms' local spin moment [121, 123]. The centroids of e_g corresponds to the L_3 and L_2 are separated by an exchange energy (Δ) $\approx$ 13 eV. The crystal field lifts the degeneracy of the $2p_{1/2}$ and $2p_{3/2}$ levels so as two levels with e_g and t_{2g} symmetry are created, as indicated by the two peaks at 710.44 eV and 712.11 eV, and at 723.60 eV and 725.31 eV with splitting energy; 1.67 eV and 1.71 eV, respectively. Fig. 6.12(b) shows the Sm-$M_{5,4}$ edge XAS spectra represent the two main peaks (M_5 and M_4) with satellites on the low energy side are clearly observed, marked with star for the sample. The main peaks of Sm at 1083.47 eV and 1108.36 eV are observed and related to the transitions from an atomic Sm^{3+} ground

state configuration. The satellite peaks may be originate from the transitions of 4f states

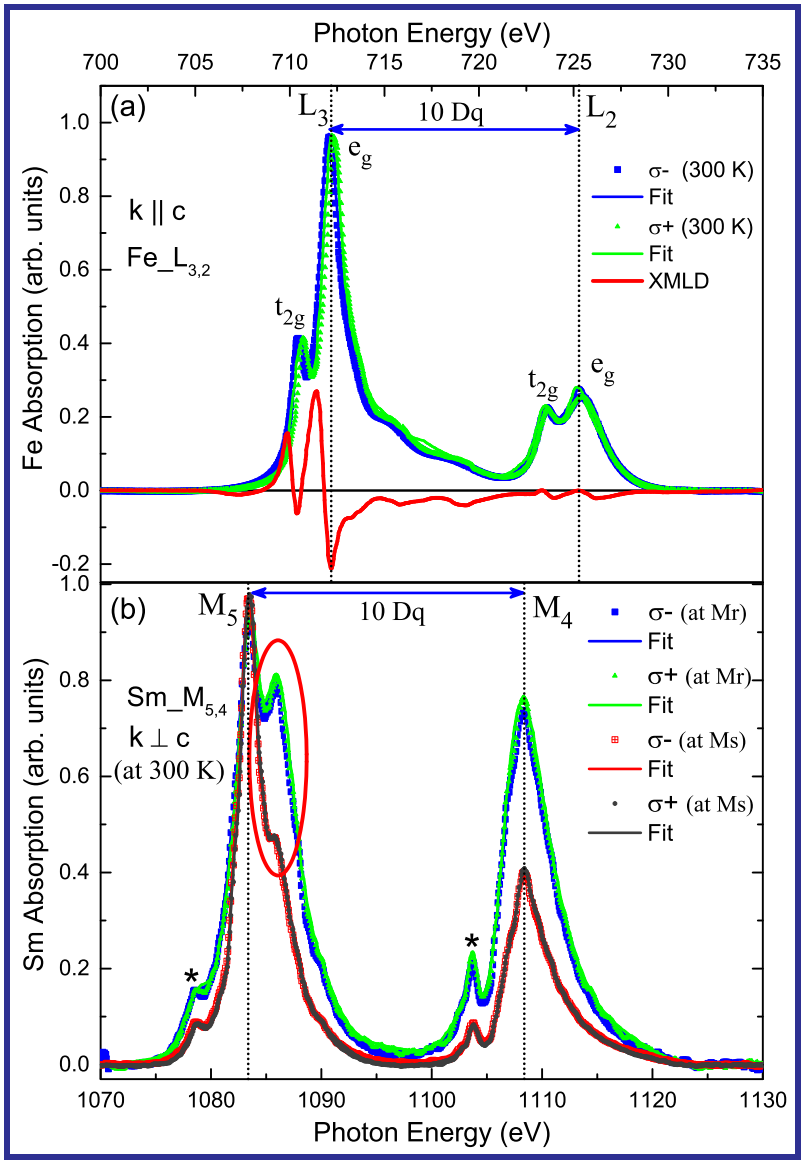

Fig. 6.12 (a) The Fe $L_{2,3}$-edge spectra of $SmFe_{3/4}Mn_{1/4}O_3$, shows Fe^{3+} state predominantly with the evolution of e_g and t_{2g} features at 300 K, and (b) Sm $M_{4,5}$-edge spectra measured on single crystal sample of SFMO, shows the significant change in multiplet features of M_5 at M_r and M_s

in the conduction band. One of the peak splits at the higher energy side of the prominent peak M_5 at M_r, which will almost vanish at saturation magnetization at room temperature.

6.5 Summary and Conclusions

In the summary, this chapter demonstrate the successful synthesis of a single phase polycrystalline SFMO perovskite oxides using solid-state reaction route method. The high-quality of single crystals were grown with four mirror optical floating zone method. Structural characterizations have been performed using XRD, TEM, HRTEM, and selected area electron diffraction pattern, and X-ray Laue diffraction. The experimental findings suggest that orthoferrite SFMO displays multiple distinct features compare with both parent compounds $SmFeO_3$. Mn^{3+}- substitution in $SmFeO_3$ (SFO) leads a new spin-reorientation transition ($\Gamma_2 \rightarrow \Gamma_1$) in the narrow window of temperature 150-180 K and significant suppression in the second order transition, called as $\Gamma_4 \rightarrow \Gamma_2$ (480 to 390K) towards the room temperature that was present in the parent's compound. The origin of SRTs is attributed to spin-phonon coupling at bulk, and at the nuclear lenght scale quantitative information is evidenced from the temperature dependence X-ray absorption spectroscopy in the SFMO single crystals. Our experimental findings pave the way for accessing the atomic scale details to understand the multi-functional behavior of SFMO crystals.